

# Flexural and shape memory properties of unidirectional glass and carbon fibers reinforced hybrid shape memory polymer composites

Hanxing Zhao<sup>1</sup>, Xin Lan<sup>1,\*</sup>, Yanju Liu<sup>2</sup> , Debes Bhattacharyya<sup>3</sup> and Jinsong Leng<sup>1,\*</sup> 

<sup>1</sup> Centre for Composite Materials and Structures, Science Park of Harbin Institute of Technology, Harbin 150080, People's Republic of China

<sup>2</sup> Department of Astronautical Science and Mechanics, Harbin Institute of Technology, Harbin 150001, People's Republic of China

<sup>3</sup> Centre for Advanced Composite Materials, Department of Mechanical Engineering, The University of Auckland, Auckland, New Zealand

E-mail: [lanxin@hit.edu.cn](mailto:lanxin@hit.edu.cn) and [lengjs@hit.edu.cn](mailto:lengjs@hit.edu.cn)

Received 11 July 2022, revised 8 September 2022

Accepted for publication 26 September 2022

Published 27 October 2022



CrossMark

## Abstract

There has been a lot of research on hybrid composites, but most of the research is limited to traditional composites. As a kind of thermo-responsive material, the mechanical properties of shape memory polymer composites (SMPCs) vary dramatically with temperature, so researches on the isothermal mechanical properties of hybrid SMPCs under different temperatures are necessary. This paper investigates the flexural and shape memory performances of carbon fiber (CF) and glass fiber (GF) reinforced hybrid SMPCs. After determining the lamina properties of CF and GF laminae at different temperatures, the flexural properties of hybrid SMPCs were predicted by simulation and theoretical calculations, which agreed well with the subsequent experimental results. The failure modes, dynamic thermomechanical properties, and shape memory properties of hybrid SMPCs with different fiber stacking configurations at different temperatures were then investigated. Finally, the effects of hybrid ratios on the flexural moduli of hybrid SMPCs at different temperatures were studied.

Supplementary material for this article is available [online](#)

Keywords: hybrid composite, shape memory polymer, flexural property, hybrid ratio, fiber stacking configuration

(Some figures may appear in colour only in the online journal)

## 1. Introduction

Shape memory polymer (SMP) can respond to external stimuli by combining and modifying its molecules [1]. The external stimulus includes heat, electric field, light, moisture, PH

changing, magnetic field, and so on [2–5]. At present, thermo-responsive SMP is the most common type, and the shape memory process can be divided into the following steps: (a) heat the SMP above its glass transition temperature ( $T_g$ ), and the material will be soft enough to bear large deformation without any damage; (b) bend the SMP to a temporary shape, such as 'U' shape and then cool down, the SMP will be hard and brittle, so the temporary shape can be fixed; (c) heat the

\* Authors to whom any correspondence should be addressed.

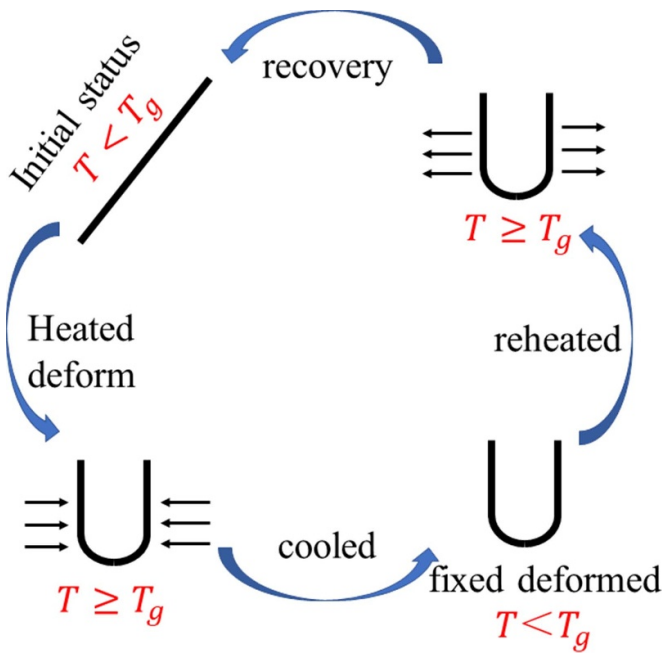


**Figure 1.** The ‘initial status-fixed deformation–restoration to initial status’ cycle of SMP.

pre-deformed SMP above its  $T_g$  again, it can recover from the temporary shape to its original shape [6–8]. The ‘initial status-fixed deformation-restoration to initial status’ cycle of SMP is shown in figure 1, and this process is repeatable [9, 10]. The recoverable strain of SMP is large, but the low tensile modulus, tensile strength, and poor thermo-mechanical properties will limit its application, especially in aerospace fields [11–16]. So, the reinforced materials, such as particles or fiber fillers are introduced into SMP to enhance its mechanical properties. The fiber reinforced shape memory polymer composites (SMPCs) have the characteristics of lightweight, high tensile modulus and strength, which can significantly improve the load carrying capacity of spacecraft, hence making the study of SMPC very necessary [12].

As for fiber fillers, carbon fibers (CFs) have excellent mechanical properties overall, but compared to the tensile strength, their average compressive strength is significantly lower, which will be a disadvantage when using carbon fiber reinforced polymer (CFRP) as a structural member under compressive or flexural conditions [15, 16]. Compared to CF, the tensile strength of glass fiber (GF) is lower, but the strain to failure and the ratio of compressive-to-tensile strengths are higher; so, the GF reinforced polymer (GFRP) may have better compressive and flexural performances than those of CFRP [17–21]. In addition to CF and GF, there are also some functional fibers, such as conductive fibers, optical fibers, nanofibers, and others, which have unique chemical or physical properties. For example, materials that are reinforced by conductive fibers can be used on the surface of the spacecraft to avoid the risk of charge concentration. To take full advantage of different types of fibers, the matrix can be reinforced by

different kinds of fibers, and thus the ‘hybrid’ composites can be manufactured [22, 23].

Dong *et al* researched the mechanical properties of CF/GF hybrid composites and showed that when there was 24% GF content in the specimen, the flexural strength was the highest [24–26]. A recent study by Yan and Cao [27] reported a novel kind of hybrid composites. The direct injection molding process was used to fabricate the GF and CF reinforced hybrid polypropylene composites, and they found that the interfacial shear strength decreased between the CF and polypropylene. Hung investigated the failure modes and responses when hybrid composites were under low-velocity impact test, and found that if the CF was used on the outer sides of a specimen, the size and deflection of damage may reduce because the strength of the bottom layer would control the flexural strength of the whole specimen [28]. There has been a lot of research on hybrid composites, but most of the research has been limited to traditional composites, and only the hybrid effects at room temperature are investigated. Besides, SMPC is a kind of thermo-responsive material, whose mechanical properties vary dramatically with temperature. As a consequence, research on the isothermal mechanical properties of hybrid SMPCs at different temperatures is very important. Besides, the effects of fiber stacking configurations on the shape memory properties of hybrid SMPCs should also be studied.

In this study, the epoxy-based SMP was used as the matrix, and the most common CF and GF were used as fiber fillers. Specimens were prepared by the hand lay-up process with different fiber stacking configurations. The isothermal uniaxial tensile tests, isothermal three-point bending tests, dynamic thermomechanical analyses (DMAs), and shape memory performance tests were all performed, and the mechanical properties of hybrid SMPCs were evaluated. The finite element method (FEM) and classical laminate theory (CLT) were used to fit the experimental results, and the results from experiments, FEM, and CLT were generally in good agreement in this work. In addition, when a specimen is bent upwards, the underside of the specimen is stretched, the upper side gets compressed, and the neutral plane gradually moves to the outboard tensile side of the cross-section from the symmetry mid-plane [7]. From this, the bending failure of the hybrid composite is complex, including tensile failure and compressive failure. So, the failure mode was investigated by the scanning electron microscope (SEM). Finally, with the help of CLT, the effects of hybrid ratios on the flexural moduli at different temperatures were also investigated. The hybrid SMPCs proposed in this paper have the following advantages: (a) compared to the traditional hybrid composite materials, they can not only be used as load-bearing materials but also be used as intelligent functional materials. (b) compared with the previously developed SMPCs, the mechanical properties and shape memory performance ( $T_g$ , shape retention and recovery ratio) can be adjusted by controlling the hybrid ratios and fiber stacking configurations instead of modifying the resin.

## 2. Experiments

### 2.1. Preparation of specimens

**2.1.1. Preparation of prepreg tapes.** In this work, shape memory epoxy resin ( $T_g = 100$  °C, Harbin Institute of Technology, China) [29] was used as matrix, Toray T300S 12 K CF (Toray Industries Inc., Tokyo, Japan) and S4C10-640 type 30 single-end continuous GF roving (Sinoma Science & Technology Co., Ltd, China) were used as the reinforcing fiber fillers. Table 1 shows the fundamental mechanical properties of fibers and cured epoxy resin. To acquire high-quality composite laminate, the technology of two-step automated tape laying was applied to manufacture CF and GF reinforced prepreg tapes (300 mm width prepreg production line, Coatema, Germany), and the detailed preparation steps are shown in section S1, supplemental information. Both the CF and GF prepreps had nominally the same resinous mass fraction of 50%. The corresponding fiber volume fractions of CF and GF prepreps can be calculated as 40% and 33%, respectively.

**2.1.2. Preparation of SMPCs.** To prepare test specimens, the prepreg tapes were arranged in unidirectional configurations and manufactured into test specimens utilizing the hand lay-up process. As shown in figure 2(a), six kinds of unidirectional fiber stacking configurations ( $C_6$ ,  $G_6$ ,  $(CG)_3$ ,  $(GC)_3$ ,  $C_3G_3$ ,  $G_3C_3$ ) were chosen in this work, and the stacking sequence was set as  $[0^\circ]_8$ . The detailed preparation process of the SMPC specimens is shown in section S2, supplemental information. It is worth noting that  $C_6$  and  $G_6$  laminates with the stacking sequence of  $[45^\circ / -45^\circ]_{48}$  were also prepared to acquire the shear moduli of the composites, according to the testing standard of American Society for Testing and Materials, ASTM D3518 [30]. By measuring the thickness of the prepared specimens, it can be calculated that the average thickness of CF lamina is  $0.223 \pm 0.00075$  mm, while for GF lamina, the average thickness is  $0.243 \pm 0.00075$  mm. After the laminates are prepared, the specimens are cut into smaller specimens with different dimensions by a water jet cutting machine (Nanjing Bitong Technology Co., Ltd, China). It should be noted that all the specimens with the same fiber stacking configurations are cut from one large laminate.

### 2.2. Isothermal uniaxial tensile tests

The lamina properties of composites, including longitudinal modulus ( $E_{11}$ ), shear modulus ( $G_{12}$ ), the Poisson's ratio ( $\nu_{21}$ ) and the transverse modulus ( $E_{22}$ ) were conducted by the isothermal uniaxial tensile tests. Table 2 shows the dimensions of specimens according to ASTM standards [30, 31]. Section S3, supplemental information details the testing procedures and calculation methods of  $E_{11}$ ,  $E_{22}$ ,  $\nu_{21}$ , and  $G_{12}$ .

### 2.3. Isothermal three-point bending test

The flexural properties were determined through three-point bending tests in this work. The depths of all the specimens

**Table 1.** Fundamental mechanical properties of the fibers and cured SMP at 25 °C.

Material	Tensile modulus (GPa)	Tensile strength (MPa)	Density ( $\text{g cm}^{-3}$ )
Toray T300S carbon fiber	230	3530	1.78
S4C10-640 glass fiber	79	3034	2.41
Epoxy resin	1.8	65.4	1.2

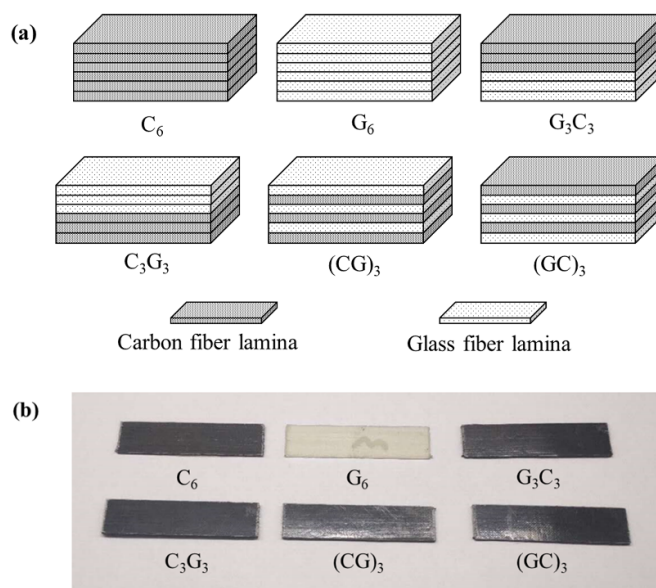


**Figure 2.** Hybrid SMPCs with different fiber stacking configurations, (a) schematic diagram of fiber stacking configurations, (b) six kinds of test specimens.

were less than 1.6 mm (ranging from 0.98 mm to 1.48 mm, depending on the fiber stacking configurations), so the dimensions of specimens were chosen to be 12.7 mm  $\times$  50.8 mm according to ASTM D790-07 [32], as shown in figure 2(b). Section S3, supplemental information details the testing procedures and calculation methods of the flexure modulus ( $E_f$ ), flexure stress ( $\sigma_f$ ) and flexural strain ( $\epsilon_f$ ).

### 2.4. Failure mode and morphology

The failure mechanism of fiber reinforced composite is rather complicated; in general, the failures always include tensile failure, compressive failure, and delamination. When a specimen is bent, two surfaces of the specimens are stretched and compressed, respectively. Besides, delamination is always caused by shear stress, which may be caused by the incorporation of CF and GF [33, 34]. As the tensile strengths and moduli of CF and GF are generally high, tensile failure is uncommon in the flexural test. While the compressive strengths and moduli of CF and GF are much lower, so compressive failure will be the most common type of failure mode in fiber reinforced composites. Different failure mechanisms may cause different

**Table 2.** The dimensions and testing standards of specimens with different stacking sequences.

Stacking sequences	Width (mm)	Length (mm)	Thickness (mm)	Testing standard
0° unidirectional	15	250	1	ASTM D3039
90° unidirectional	25	175	2	ASTM D3039
±45° balance and symmetric	25	250	2.5	ASTM D3518

failure modes, such as fiber splitting, fiber buckling, kink bands, fiber crushing, and so on. So, in this work, to determine the failure modes of hybrid SMPCs with different fiber stacking configurations, an SEM (Nippon Corporation, Japan) was used.

### 2.5. DMA test

DMA is an effective testing method to characterize the relationship between the mechanical properties and time, temperature, or frequency of viscoelastic materials. Compared with the isothermal mechanical test, the dynamic thermomechanical test can reflect the performance of the material under actual conditions more accurately, and only a small amount of specimen is needed. To determine the dynamic thermomechanical properties of the SMPC specimens, a TA instrument DMA Q800 machine was used in this work, and the clamp arrangement was chosen to be three-point bending with a span of 50 mm. The frequency mode was set to be the multi-frequency mode with the frequency of 1.0 Hz, and the temperature ranged from 25 °C to 150 °C with a heating rate of 5 °C min<sup>-1</sup>. According to ASTM D5023-15, the dimensions of the SMPC specimens were 60 mm × 5 mm × 2 mm [35]. There were five specimens for each testing condition, and the mean values of the test data were calculated to represent the results.

### 2.6. Shape memory performance test

The shape memory properties of specimens with different fiber stacking configurations were evaluated by a universal mechanical testing machine Zwick Z010. The testing method and calculating method of shape retention and recovery ratio of SMPC in this paper are referred to [29]. The specimens were incised into a rectangular shape, and the dimensions were 60 mm × 10 mm × 1.5 mm. Figure 3 showed the four steps of the shape memory performance test: (a) an oven was used to heat the specimen to 100 °C, and then the loading nose dropped to bend the material. The initial maximum deflection of the specimen was set to be  $h_0$ ; (b) after cooling down to 25 °C, the temporary shape of the specimen could be fixed; (c) rising the loading nose to its initial position (the deflection of the loading nose was zero) and the fixed deflection of the specimen  $h_f$  was measured; and (d) the specimen was reheated to 100 °C quickly and the residual deflection  $h_r$  was measured. The complete thermomechanical loading programming was shown in figure 3. The corresponding initial maximum deflection ( $\varepsilon_0$ ), fixed deflection ( $\varepsilon_f$ ) and residual deflection ( $\varepsilon_r$ ) were calculated by equation (S.9). It should be noted that  $\varepsilon_0$

was chosen to be 1% in this section. This was mainly because the specimens began to suffer major failure or breakage when the strain was greater than 2% observed in the isothermal three-point bending tests. Hence, no specimens were used at more than half of the breaking strain to provide a minimum safety factor of 2.

The shape fixity ratio was defined as [29]:

$$R_f = \frac{\varepsilon_f}{\varepsilon_0} \times 100\% \quad (1)$$

and the shape recovery ratio was defined as [29]:

$$R_r = \frac{\varepsilon_0 - \varepsilon_r}{\varepsilon_0} \times 100\%. \quad (2)$$

There were at least five specimens for each testing condition, and the mean values of the test data were calculated to represent the results.

## 3. Simulation and theoretical analysis of hybrid SMPCs

### 3.1. Finite element analysis (FEA)

The distribution of stress and deflection were analyzed by a commercial software package Abaqus 6.12, which was helpful to better understanding the flexural process of hybrid composites. For simplification, the applied stress in the FEA model was regarded as 1 MPa, and the range of the applied stress is 1 mm in the middle of the specimen. Because the boundary conditions of the FEA model were symmetric, we can only model half of the laminate, and the boundary conditions and dimension of the model are shown in figure 4. The element type was S4R element, and the mesh size was 0.25 mm × 0.25 mm.

The lamina properties were defined separately as CF lamina and GF lamina, and the stacking configurations of  $C_6$ ,  $G_6$ ,  $(CG)_3$ ,  $(GC)_3$ ,  $C_3G_3$ ,  $G_3C_3$  were defined separately in Abaqus®. The lamina properties  $E_{11}$ ,  $E_{22}$ ,  $\nu_{21}$  and  $G_{12}$  could be obtained from the tensile test, and  $G_{13}$ ,  $G_{23}$  could be derived by Hashin's model [24]. The shear modulus of SMPC can be regarded as irrelevant to the reinforced fibers, so the following assumptions can be proposed:  $G_{12} = G_{13} = G_{23}$ . Figure 5 shows the deformed contour of the  $C_6$  specimen. The maximum deflection under the applied force can be read from the FEA results, so the flexural modulus can be obtained by using the deflection  $\delta$  through equation (S.8).



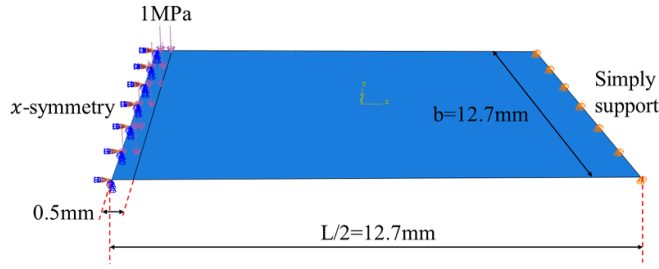


**Figure 4.** FEA model of the three-point bending specimen (only model half of the laminate).

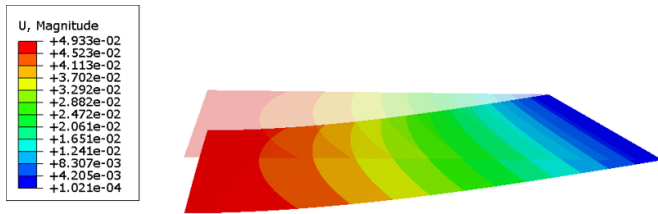


**Figure 5.** FEA result of the  $C_6$  specimen (the deformation scale factor is 30).

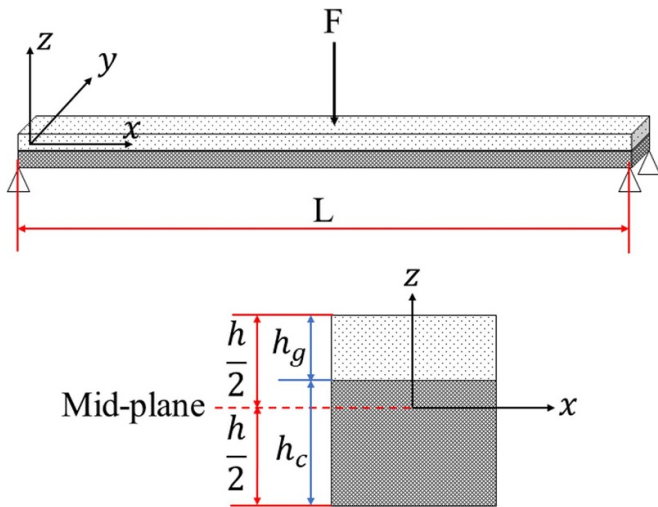


**Figure 6.** The coordinate system of the laminate under three-point bending condition ( $g$  and  $c$  represent the GF and CF reinforced laminates, respectively).

### 3.2. The theoretical analysis

The coordinate system of the laminate under the three-point bending condition is established as shown in figure 6. The  $xy$  axes are in the mid-plane of the laminate geometrically, and the  $z$  axis defines the direction of thickness.

The strain in the coordinate system of laminate can be written as follow, according to the CLT:

$$\varepsilon = \varepsilon^0 + z\kappa \quad (3)$$

where  $\varepsilon^0$  and  $\kappa$  are expressed as equations (S.10) and (S.11).

The relationship between stress matrix and the strain matrix are shown in equation (S.12). As for the three-point bending specimen,  $N = 0$  and  $M_y = M_{xy} = 0$ , so it can be simplified as:

$$\begin{Bmatrix} \mathbf{0} \\ \mathbf{M} \end{Bmatrix} = \begin{bmatrix} \mathbf{A} & \mathbf{B} \\ \mathbf{B} & \mathbf{D} \end{bmatrix} \begin{Bmatrix} \varepsilon^0 \\ \kappa \end{Bmatrix} \quad (4)$$

where

$$\mathbf{M} = [M_{xx} \quad 0 \quad 0]^T \quad (5)$$

The stress matrix and curvature matrix of mid-plane  $\varepsilon^0$  and  $\kappa$  are:

$$\varepsilon^0 = \mathbf{B}_1 \mathbf{M} \quad (6)$$

$$\kappa = \mathbf{D}_1 \mathbf{M} \quad (7)$$

where

$$\mathbf{B}_1 = -\mathbf{A}^{-1} \mathbf{B} (\mathbf{D} - \mathbf{B} \mathbf{A}^{-1} \mathbf{B})^{-1} \quad (8)$$

$$\mathbf{D}_1 = (\mathbf{D} - \mathbf{B} \mathbf{A}^{-1} \mathbf{B})^{-1} \quad (9)$$

As shown in figure 6, the internal moment  $M_{xx}$  is no constant, which changes with the  $x$  direction: when  $x = L/2$ ,  $M_{xx}$  reaches its maximum,  $-FL/4$ , while when  $x = 0$  and  $x = L$ ,  $M_{xx} = 0$ . When  $x = L/2$ , the stress also reaches its maximum. The deflection at the mid-span can be calculated as follow [36]:

$$w_0 = -\frac{\kappa_{xx \max} L^2}{3}. \quad (10)$$

Then, the flexural modulus can be obtained using equation (S.7).

## 4. Results

### 4.1. The lamina properties

The longitudinal modulus  $E_{11}$  of CF and GF reinforced SMPCs at different temperatures are shown in figure 7. It is clear that the longitudinal modulus of CFRP is about 2 or 3 times higher than that of GFRP. With the increase in temperature,  $E_{11}$  of both CFRP and GFRP decrease monotonically. The longitudinal modulus of CF reinforced SMPC is 40 653 MPa at 25 °C and 16 676 MPa at 100 °C, while for GF reinforced SMPC, this modulus is 16 867 MPa at 25 °C and 7668 MPa at 100 °C. It is worth noting that when the temperature changes from 25 °C to 100 °C,  $E_{11}$  only drops to about 40% of the original value, and the SMPCs will not lose the axial load carrying capacity. The reason for this phenomenon is the introduction of reinforced fibers increased the load carrying capacity of SMPC along the fiber direction. Although the resin matrix changes from glassy state to rubber state and loses its load carrying capacity when the temperature is above  $T_g$ , the reinforced fibers can still bear a considerable load. Therefore, the fibers can significantly enhance the longitudinal mechanical properties of the SMPC. It should be noted that, in the tensile

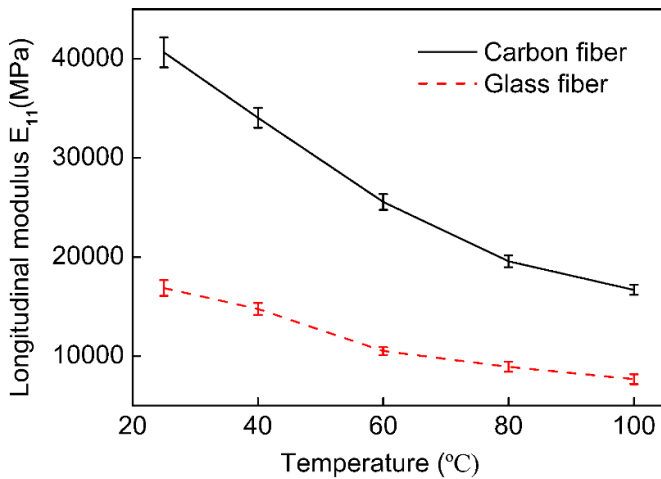


**Figure 7.**  $E_{11}$  of CF and GF reinforced SMPCs at different temperatures.

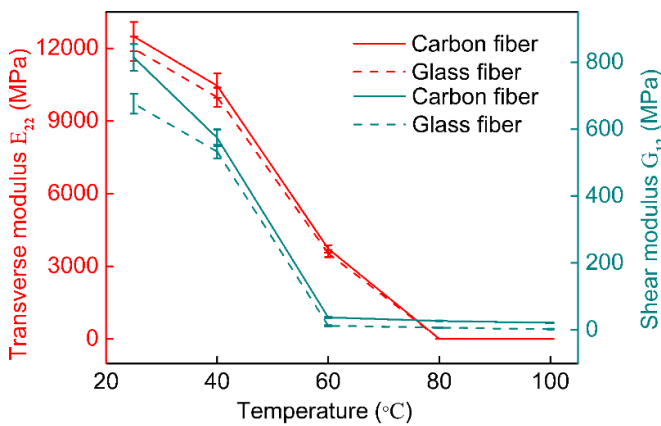


**Figure 8.**  $E_{22}$  and  $G_{12}$  of CF and GF reinforced SMPCs at different temperatures.

process, the displacement of the fiber cannot be equal to the one of the SMP, because the fibers are not completely straight in the longitudinal direction due to the limitations in the manufacturing processes. Therefore, the  $E_{11}$  obtained from the experiment will be lower than that from the mixture rule.

The transverse moduli and shear moduli at different temperatures for CF and GF reinforced SMPCs are shown in figure 8. Different from the longitudinal mechanical properties of SMPC, the transverse and shear moduli of CF reinforced SMPC are almost the same as those of GF reinforced SMPC, and it drops sharply when the temperature increases. Because the transverse and shear moduli of SMPC are mainly related to the matrix, which are almost independent of the reinforced fibers. Unlike the 60% decrease in longitudinal modulus, when the temperature changes from 25 °C to 100 °C, the  $E_{22}$  and  $G_{12}$  drop to about 0.07% and 0.3% of the original value, respectively. This means that the reinforced fibers cannot enhance the transverse and shear mechanical properties of SMPC. When the resin matrix changes from the glassy state to rubbery state, the SMPC will lose its transverse and shear loads bearing capacities. The lamina properties of CF and GF

reinforced composites at different temperatures are listed in table 3.

#### 4.2. Flexural moduli of hybrid SMPCs at different temperatures

Figure 9 shows the flexural moduli of hybrid SMPCs with different fiber stacking configurations as a function of temperature from experiments, FEA and CLT. The results are generally consistent except for exceptions in some specific data. It is shown that the flexural moduli decrease with the increase of temperature for all stacking configurations. With the increase in temperature, the resin matrix of SMPC will change from glassy state to rubbery state, thus, the SMPCs will become softer. Besides, the flexural moduli decrease rapidly when the temperature rises from 40 °C to 80 °C and keep at an extremely low value with a further increase of temperature from 80 °C to 100 °C. Therefore, the SMPC will lose its flexural resistance completely when the temperature is higher than 80 °C.

The flexural moduli of SMPCs as a function of fiber stacking configurations at different temperatures are shown in figure 10. It is seen that under all temperature conditions, CF reinforced SMPCs have the highest flexural moduli, while GF reinforced SMPCs have the lowest flexural moduli. This trend is similar to the tensile moduli of CF and GF reinforced SMPCs at different temperatures, shown in table 3. As for  $C_3G_3$ ,  $G_3C_3$ ,  $(CG)_3$  and  $(GC)_3$ , although the volume fraction of each fiber component is the same, the flexural moduli are quite different. The flexural moduli of  $(CG)_3$  and  $(GC)_3$  are always higher than those of  $C_3G_3$  and  $G_3C_3$ . Because when the SMPC is bent, one side of the laminate is stretched while the other side is compressed, resulting in the difference of tensile and compressive modulus of the adjacent lamina having a great influence on the hybrid effect. For  $(CG)_3$  and  $(GC)_3$ , the flexural moduli between every adjacent lamina are different, so large hybrid effect exists and the flexural moduli will be higher than that of  $C_3G_3$  and  $G_3C_3$ . It is worth noting that under all temperature conditions, the flexural moduli of  $C_3G_3$  and  $(CG)_3$  are slightly higher than those of  $G_3C_3$  and  $(GC)_3$ . From which we can see that specimens with carbon lamina on the tensile side will have higher flexural modulus than specimens with carbon lamina on the compressive side. For SMPCs with different fiber stacking configurations, positive effects can always be found in the hybrid composites.

#### 4.3. DMA results

As revealed in figure 11(a), when the temperature is relatively low, the storage moduli of all six kinds of SMPCs maintain relatively high values, so the SMPCs will stay in the 'hard' state. When the temperature rises, there will be a rapid decrease in the storage modulus and then remains stable, because the storage modulus of SMP materials will change drastically around  $T_g$ . At relatively low temperature, the storage modulus of  $C_6$  and  $G_6$  are 47 216 MPa and 15 591 MPa, respectively. While when the temperature rises above  $T_g$ , the storage moduli will stabilize at 1720 MPa and 343 MPa for  $C_6$  and  $G_6$ , respectively.

**Table 3.** The lamina properties of CF and GF reinforced composites at different temperatures.

Temperature (°C)		25	40	60	80	100
CF reinforced SMPC	$E_{11}$ (MPa)	40 653	34 053	25 559	19 558	16 676
	$E_{22}$ (MPa)	12 491	10 460	3732	17.3	9.04
	$\nu_{21}$	0.29	0.77	0.63	0.44	0.41
	$E_{45}$ (MPa)	3031	2195	148	42.3	25.4
	$G_{12}$ (MPa)	814	574	37.4	27.2	21.2
GF reinforced SMPC	$E_{11}$ (MPa)	16 867	14 753	10 500	8912	7668
	$E_{22}$ (MPa)	11 987	9985	3540	16.5	8.6
	$\nu_{21}$	0.34	0.89	0.38	0.42	0.4
	$E_{45}$ (MPa)	2528	2081	49.7	19.7	7.4
	$G_{12}$ (MPa)	675.9	533.4	12.5	7.02	2.36

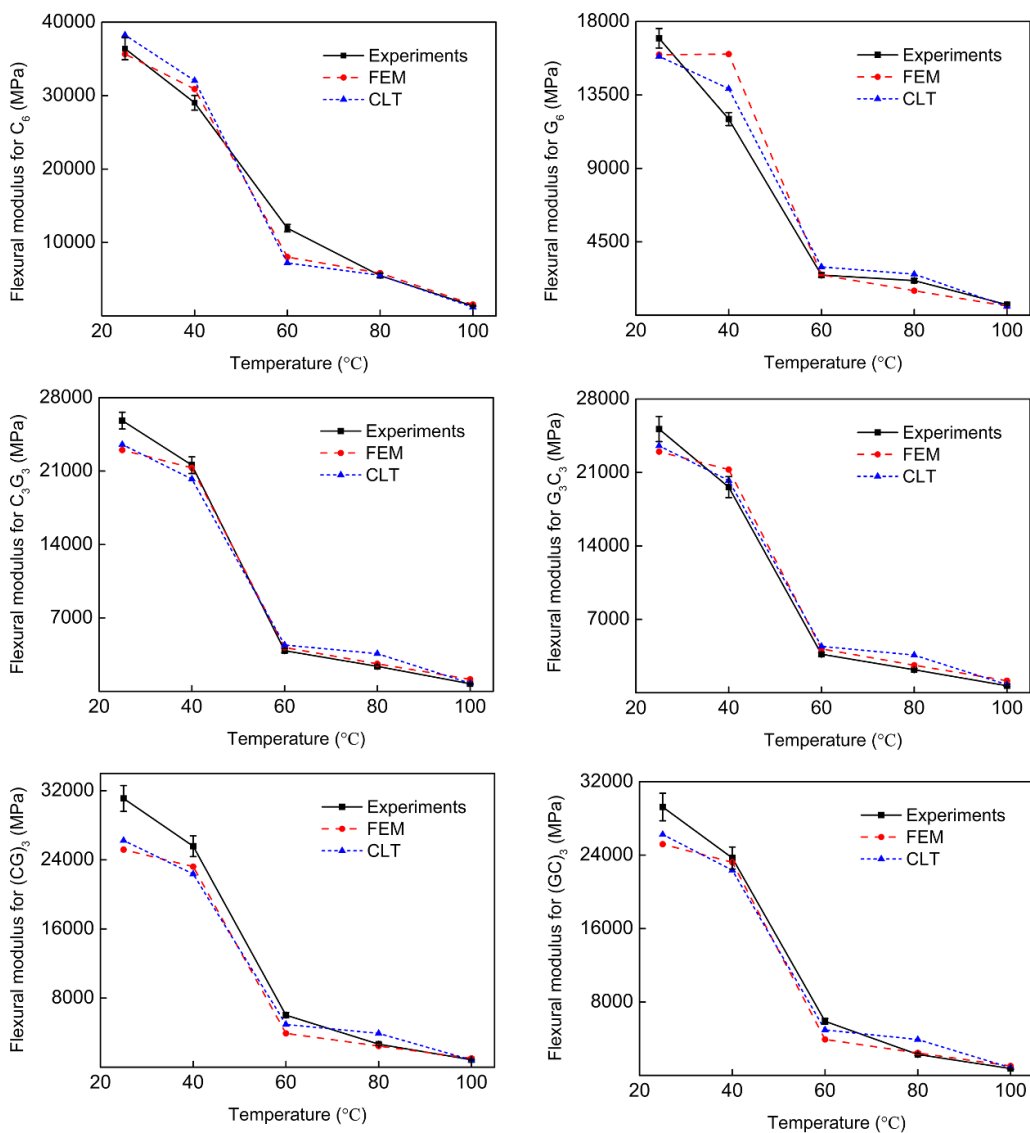
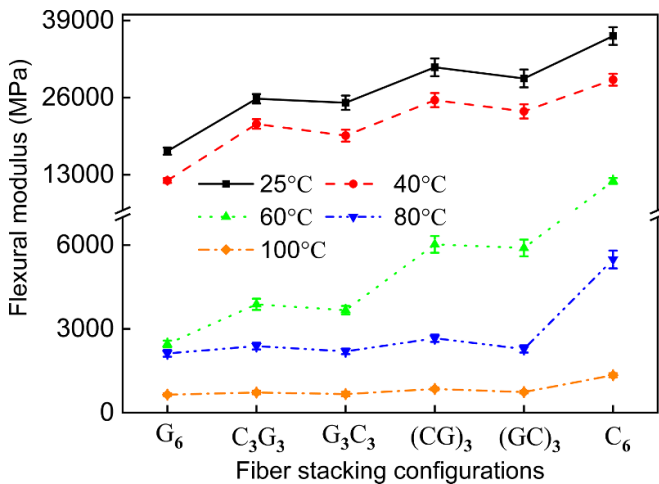
**Figure 9.** Flexural moduli of hybrid SMPCs with different stacking configurations as a function of temperatures from experiments, FEA and CLT.

Figure 11(b) is the Temperature-Tan Delta curve of hybrid SMPCs with different fiber stacking configurations, which represents the viscoelastic properties of the specimens. When

the loss factor of material is larger, the material will be more viscous; conversely, the material will be more elastic. The temperature corresponding to the peak of the Temperature-Tan



**Figure 10.** Flexural moduli of SMPCs at different temperatures as a function of fiber stacking configurations from experiments.

Delta curve is regarded as the  $T_g$  of the SMPC. Figure 11(b) indicates that  $G_6$  has the highest  $T_g$  of about 95 °C, while  $C_6$  has the lowest  $T_g$  of about 67 °C. The glass transition temperatures of  $C_3G_3$ ,  $G_3C_3$ ,  $(CG)_3$  and  $(GC)_3$  are 70 °C, 69 °C, 74 °C and 73 °C, respectively, which keep at almost the same level. The reason for this phenomenon is as follows: CF has better thermal conductivity than that of GF, so the thermal conductivity of  $C_6$  is the best, and it can reach its glass transition temperature faster during heating. Therefore, the  $T_g$  of  $C_6$  will be lower than that of  $G_6$ . The thermal conductivities of  $C_3G_3$ ,  $G_3C_3$ ,  $(CG)_3$  and  $(GC)_3$  are almost the same, so their glass transition temperatures will keep at the same level.

#### 4.4. Failure morphology

The micrograph images of a representative SMPC laminate at different temperatures are shown in figure 12, where the flexural strain of all the specimens is the same (2%). It is worth noting that there is no significant difference in the morphologies for all the specimens with different fiber stacking configurations at the same temperature, so  $C_6$  is chosen as representation. When the specimens are bent under different temperatures, different kinds of damages may occur. It is seen that under 25 °C, the failure mechanism may be the shear failure mode. The kink bands can be found on the compressive side of specimens, while the fiber pullout and fiber splitting can be found on the tensile side. When shear damage occurred in the specimen, there will be additional displacements, so the calculated flexural modulus may be lower than the actual value [18]. As for specimens under 40 °C, there exist fiber buckling on the compressive side and slight fiber pullout on the tensile side, and the resin crack can also be found on the tensile side. It is clear that with the increase in temperature, the shear failure will become lighter under the same flexural strain. When the temperature increasingly reaches 60 °C, there only exist surface wrinkles on the compressive side, without any damage in the fiber and resin. At that temperature, the tensile surface remains intact and smooth. When the temperature is further

increased to 80 °C and 100 °C, there will be no damage on both sides of the specimens, therefore, the micrograph image of SMPC under 80 °C and 100 °C are not included in figure 12.

#### 4.5. Shape memory properties

Figures 13–15 show the stress–strain, stress–temperature and strain–temperature relationships, respectively. All the curves have been smoothed and then divided into four sections, which are corresponding to the four steps in section 2.6.

Figure 13 shows the stress–strain relationships of SMPC specimens with different fiber stacking configurations. There exist significant differences in the loading slope 1 of different fiber stacking configurations. The magnitudes of the slopes of the loading curves 1 represent the flexural moduli of different specimens at 100 °C, which showed the same comparative result in section 4.2. The unloading slopes 3 of  $G_6$  and  $C_3G_3$  also show significant differences, while for  $C_6$ ,  $(GC)_3$ ,  $(CG)_3$  and  $G_3C_3$ , the unloading slopes did not depict significant variation. Although  $\varepsilon_0$  is maintained to be 1%,  $\varepsilon_f$  changes severely among different specimens:  $\varepsilon_f = 0.98\%$  for  $G_6$ ,  $\varepsilon_f = 0.965\%$  for  $G_3C_3$ ,  $\varepsilon_f = 0.933\%$  for  $C_3G_3$ ,  $\varepsilon_f = 0.922\%$  for  $(GC)_3$ ,  $\varepsilon_f = 0.919\%$  for  $(CG)_3$  and  $\varepsilon_f = 0.9\%$  for  $C_6$ . The differences in loading slopes, unloading slopes and  $\varepsilon_f$  of hybrid SMPC specimens with different fiber stacking configurations are presumably caused by the differences in flexural moduli. With the increase of flexural moduli, the shape fixity ratios of SMPCs will decrease.

The curves of stress–temperature and strain–temperature of hybrid SMPCs are shown in figures 14 and 15, respectively. The four steps in figures 14 and 15 are corresponding to the four steps in figure 13. It is worth noting that although  $G_6$  has the largest shape fixity strain ( $\varepsilon_f = 0.986\%$ ) and  $C_6$  has the lowest shape fixity strain ( $\varepsilon_f = 0.9\%$ ), as for the residual strain  $\varepsilon_r$ , there is an opposite conclusion ( $\varepsilon_r = 0.012\%$  for  $G_6$  and  $\varepsilon_r = 0.14\%$  for  $C_6$ ). That may be caused by the fact that  $C_6$  has the largest maximum stress (13.6 MPa), while  $G_6$  has the lowest maximum stress (3.92 MPa). So, the hardening of SMPCs may result in reducing the efficiency of shape recovery performance, thus reducing the shape recovery ratio.

The shape fixity ratio  $R_f$  and shape recovery ratio  $R_r$  of SMPCs with different fiber stacking configurations are shown in figure 16. The  $R_f$  obtained for  $G_6$ ,  $G_3C_3$ ,  $C_3G_3$ ,  $(GC)_3$ ,  $(CG)_3$  and  $C_6$  are 98.6%, 96.5%, 93.3%, 92.2%, 91.9% and 90%, respectively, at 25 °C; while  $R_r$  are 98.8%, 97.4%, 95.7%, 93.3%, 91.8% and 86%, respectively, at 100 °C.  $G_6$  has the best shape memory ability, while  $C_6$  has the worst. These results reveal that the shape memory abilities of unidirectional hybrid SMPCs are excellent, and the flexural modulus may have great effects on them. The reason for this phenomenon is that the shape memory effect of SMPCs is determined by the micro-Brownian motion of soft segments of the shape memory resin, and the reinforcing fiber may reduce the activity of the resin. When the fiber is harder, the effect is more severe. During the shape fixity and recovery processes of SMPC, if the fiber is harder (that is the flexural modulus is higher), the micro-Brownian motion of the SMP will become less active, and hence the  $R_r$  and  $R_f$  will be lower. That is why the shape

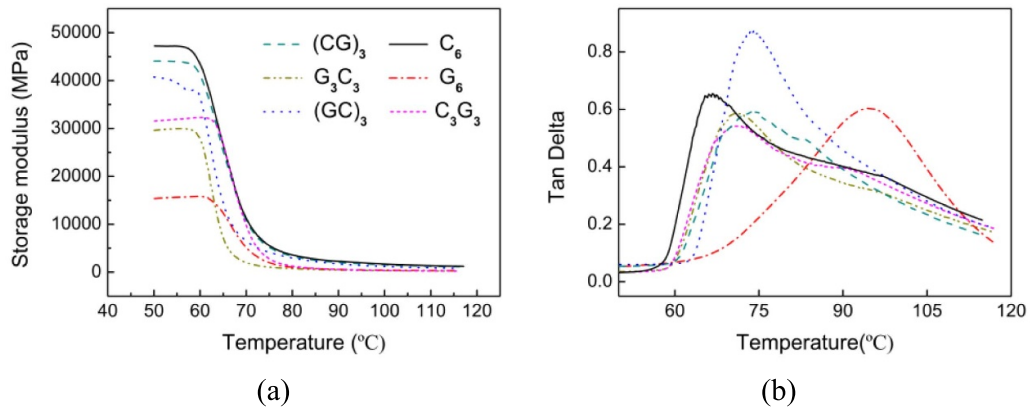


Figure 11. DMA testing results of hybrid SMPCs, (a) storage modulus, (b) Tan Delta.

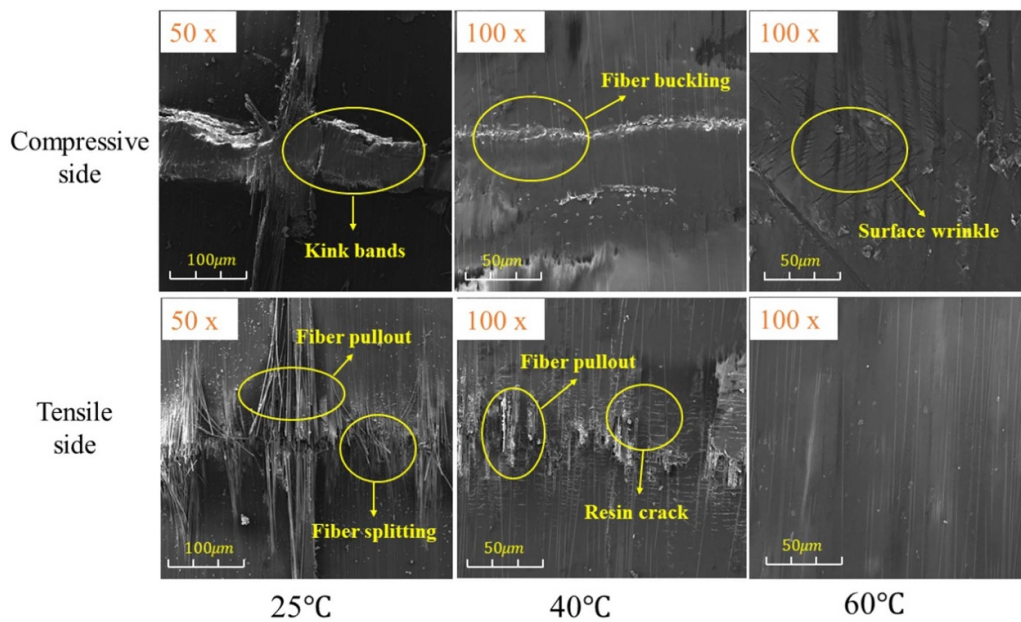


Figure 12. Morphologies of both sides of hybrid SMPC specimens at different temperatures.

fixity and recovery ratios of SMPC will reduce as its flexural modulus increases.

## 5. The effect of hybrid ratio and some inferences

Through the above research, it can be seen that the fiber stacking configurations have a great influence on the flexural and shape memory properties of hybrid SMPCs, but the effect of hybrid ratio has not been investigated. In this section, the CLT is used to calculate the flexural properties of hybrid SMPCs with different hybrid ratios at different temperatures. To eliminate the influence of stacking configurations on the hybrid SMPCs, CF lamina and GF lamina were laid on the bottom and upper side of the composite, respectively. The ply number was also chosen to be six. As shown in figure 17, there are seven kinds of hybrid SMPCs with different hybrid ratios, and the hybrid ratios vary from 0 to 1. The normalized flexural modulus  $\eta$  was introduced to simultaneously study the effect

of hybrid ratio and temperature on the flexural properties of hybrid composites

$$\eta = E_a/E_C, \quad (11)$$

where  $E_a$  is the actual flexural modulus of the hybrid SMPC, and  $E_C$  represents the flexural modulus of  $C_6$  at 100 °C. The calculation results are shown in figure 18. We can see that with the increase of hybrid ratio (increase the number of GF lamina), the flexural modulus of the composite decreases, and this tendency is non-linear. This phenomenon is different from the result of classical hybrid theory, where the flexural modulus of hybrid composites varies linearly with the change of hybrid ratio. As shown in figure 18, the flexural modulus of hybrid SMPC will decrease rapidly with the introduction of GF lamina, and once the content of GF exceeds 30%, the further introduction of GF lamina will have little effect on the flexural modulus. However, as the hybrid ratio increases to more than 80%, there will be a sharp decline in the flexural modulus of hybrid

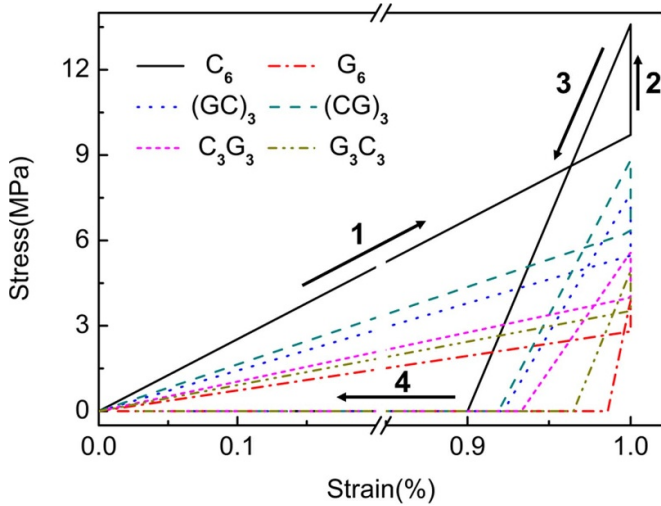


**Figure 13.** Comparison of stress vs. strain curves for SMPC with different fiber stacking configurations (1-deformation, 2-cooling/fixation, 3-unloading, 4-heating/recovery).

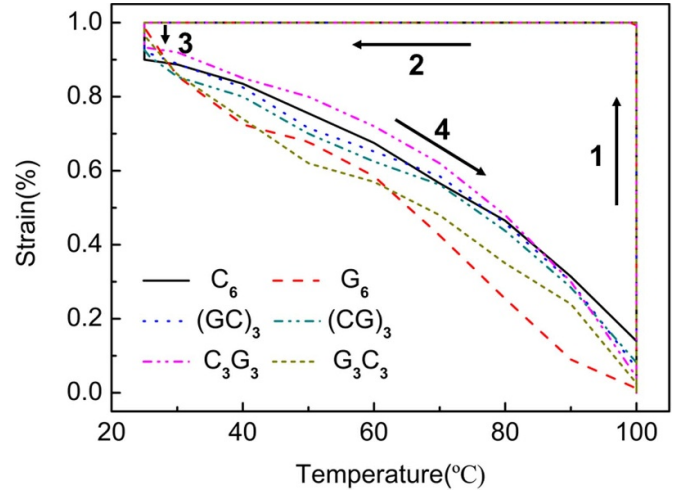


**Figure 15.** Comparison of strain vs. temperature curves for SMPC with different fiber stacking configurations (1-deformation, 2-cooling/fixation, 3-unloading, 4-heating/recovery).

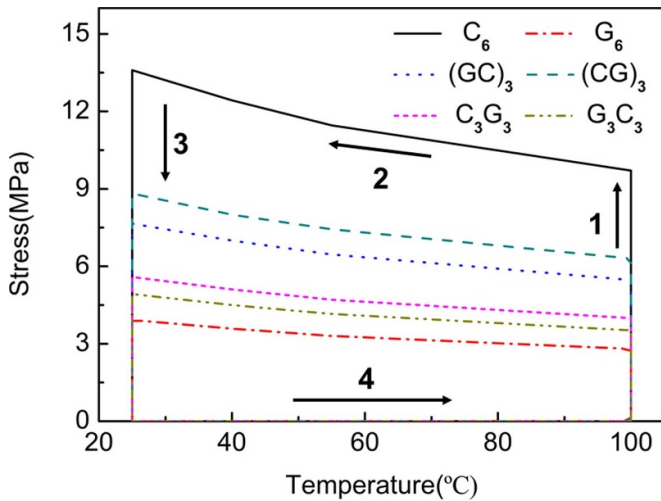


**Figure 14.** Comparison of stress vs. temperature curves for SMPC with different fiber stacking configurations (1-deformation, 2-cooling/fixation, 3-unloading, 4-heating/recovery).

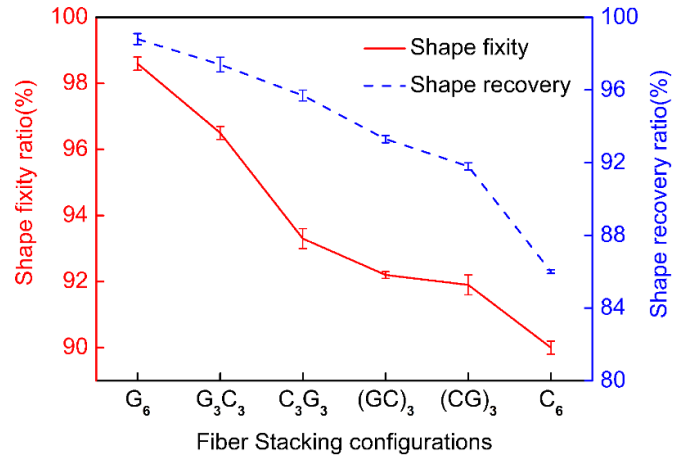


**Figure 16.** Shape fixity and recovery ratios of hybrid SMPCs with different fiber stacking configurations.

SMPCs. The above rules are applicable to this kind of unidirectional hybrid SMPCs at all temperatures. In addition, the flexural modulus of the hybrid SMPCs with the same hybrid ratio will decrease rapidly with the increase of temperature, especially from 40 °C to 60 °C, which is consistent with the above research results and also reflects the reliability of the calculation results in this section.

The following inferences can be made after the above series of experimental and theoretical verifications:

- (a) For the unidirectional interlaminar CF/GF reinforced hybrid SMPCs, the  $T_g$  can be adjusted by controlling the hybrid ratio. With the increase of the number of CF laminae, the thermal conductivity of the SMPC will increase, which will lead to the decrease of  $T_g$ .

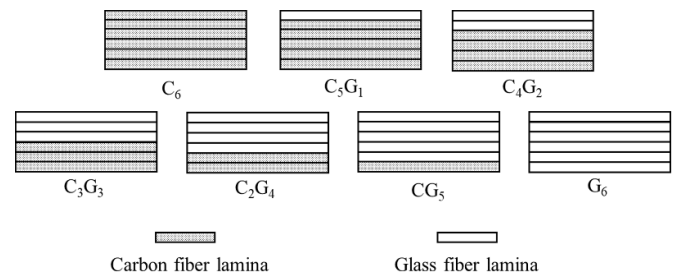


**Figure 17.** Hybrid SMPCs with different hybrid ratios.

- (b) At a certain hybrid ratio, the flexural modulus of SMPC will increase with the increase of the number of CF/GF interfaces.
- (c) The flexural modulus of hybrid SMPCs will decrease with the increase of hybrid ratio (the number of CF lamina), and this trend is non-linear.

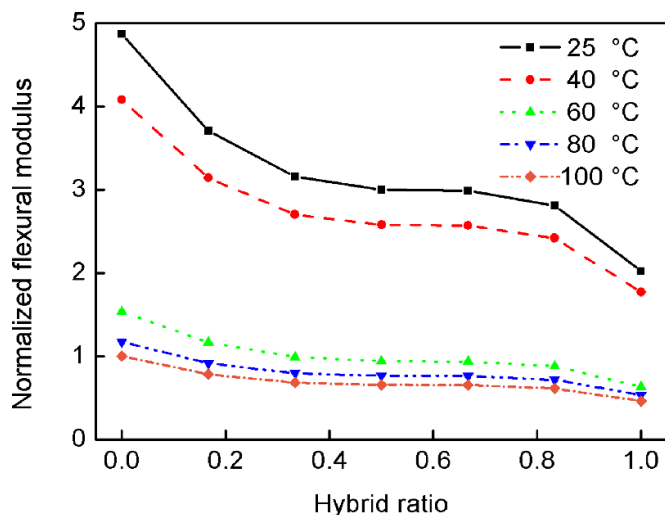


**Figure 18.** The normalized flexural modulus of hybrid SMPCs with different hybrid ratios at different temperatures.

- (d) From the shape memory testing results, the shape fixity and recovery ratios of hybrid SMPCs will decrease with the increase of their flexural modulus.
- (e) By designing the hybrid ratios and fiber stacking configurations of the interlaminar hybrid SMPCs, the flexural stiffness and shape memory properties can be regulated, which has certain guiding significance to the research on the mechanical properties of SMPCs. For example, reducing the hybrid ratio of GF lamina can improve the flexural stiffness of the hybrid SMPC, and at the same time, the  $T_g$  as well as the shape fixity and recovery ratios of the SMPC will decrease. Therefore, how to improve the flexural stiffness of hybrid SMPCs without reducing the shape memory properties by controlling the hybrid ratios and fiber stacking configurations is our future research objective.

## 6. Conclusions

This research presents the flexural and shape memory properties of unidirectional CF and GF reinforced hybrid SMPCs. Totally six kinds of SMPCs with different fiber stacking configurations are manufactured. The flexural moduli of hybrid SMPCs at different temperatures are tested by isothermal three-point bending experiments, and the experimental data show a satisfactory agreement with the results from FEA and CLT. The flexural modulus will decrease with the increase in temperature, and positive hybrid effects can always be found in the hybrid SMPCs. SEM and DMA experiments are then conducted, and the compressive failure is observed to be the dominant failure mode. From the DMA results, the full GF composite has the highest  $T_g$ , while the full CF composite has the lowest  $T_g$ , and the glass transition temperatures of  $C_3G_3$ ,  $G_3C_3$ ,  $(CG)_3$  and  $(GC)_3$  are almost at the same level.

The shape memory properties of hybrid SMPCs are also determined through shape memory performance tests. The experimental results show that the hardening of SMPCs can result in reducing the shape fixity and recovery ratios. The

full GF composite has the best shape memory performance (98.6% shape fixity ratio and 98.8% shape recovery ratio, respectively), while the full CF composite has the worst (90% shape fixity ratio and 86% shape recovery ratio, respectively). Finally, with the help of CLT, the effects of hybrid ratio on the flexural modulus of hybrid SMPC at different temperatures are investigated, and some inferences are made. With the increase in hybrid ratio, the flexural modulus of the composite will decrease, and this tendency is non-linear. When the hybrid ratio is between 30 and 80%, the further introduction of GF lamina will have little effect on the flexural modulus; while as the hybrid ratio increases to more than 80%, there will be a sharp decline in the flexural modulus of hybrid SMPCs at all temperatures. This research can be used to optimize the key parameters of hybrid SMPCs, such as the overall thickness, fiber content and hybrid ratio, so that the mechanical properties and shape memory performance can be designed by controlling the fiber stacking configurations and hybrid ratios instead of modifying the SMP. This is an integrated design, preparation and evaluation method to obtain 'requirements-functional decomposition-structure design-preparation process-performance verification'.

## Data availability statement

All data that support the findings of this study are included within the article (and any supplementary files).

## Acknowledgments

The author would like to thank for the Heilongjiang Touyan Innovation Team Program. This work is supported by the National Natural Science Foundation of China (Grant Nos. 11632005 and 11872020).

## ORCID iDs

Yanju Liu  <https://orcid.org/0000-0001-8269-1594>

Jinsong Leng  <https://orcid.org/0000-0001-5098-9871>

## References

- [1] Xie F, Gong X, Huang L, Leng J, Liu Y and Liu Y 2017 Effects of accelerated aging on thermal, mechanical and shape memory properties of cyanate-based shape memory polymer: i vacuum ultraviolet radiation *Polym. Degrad. Stab.* **138** 91–97
- [2] Gu J, Zhao S, Zhang X, Cai Z and Sun H 2020 A hygro-thermo-mechanical constitutive model for hydrothermally activated shape memory polymers under finite deformations *Mech. Mater.* **150** 103594
- [3] Jang H, Hong S, Kim J, Goo N, Lee H and Yu W 2019 Long-term properties of carbon fiber-reinforced shape memory epoxy/polymer composites exposed to vacuum and ultraviolet radiation *Smart Mater. Struct.* **28** 11
- [4] Qi Y, Sun B, Gu B and Zhang W 2022 Electrothermally actuated properties of fabric-reinforced shape memory polymer composites based on core-shell yarn *Compos. Struct.* **292** 115681

- [5] Bouaziz R, Roger F and Prashantha K 2017 Thermo-mechanical modeling of semi-crystalline thermoplastic shape memory polymer under large strain *Smart Mater. Struct.* **26** 055009
- [6] Xu L, Zhao J, Shi M, Liu J and Wang Z 2022 Thermodynamic properties of TPI shape memory polymer composites reinforced by GO/SiO<sub>2</sub> modified carbon fiber *Compos. Sci. Technol.* **226** 109551
- [7] Gu J, Zeng H, Cai Z and Sun H 2020 Modeling and laminated carbon fiber reinforced shape memory polymer composite by using a refined plate theory *Smart Mater. Struct.* **29** 095005
- [8] Zhang F, Xia Y, Liu Y and Leng J 2020 Nano/microstructures of shape memory polymers: from materials to applications *Nanoscale Horiz.* **5** 1155–73
- [9] Delaey J, Dubrueel P and Van V S 2020 Shape-memory polymers for biomedical applications *Adv. Funct. Mater.* **226** 147–75
- [10] Roudbarian N, Baniasadi M, Ansari M and Baghani M 2019 An experimental investigation on structural design of shape memory polymers *Smart Mater. Struct.* **28** 9
- [11] Guo Y, Liu Y, Liu J, Zhao J, Zhang H and Zhang Z 2020 Shape memory epoxy composites with high mechanical performance manufactured by multi-material direct ink writing *Composites A* **135** 105903
- [12] Quadrini F, Bellisario D, Iorio L and Santo L 2019 Shape memory polymer composites by molding aeronautical prepregs with shape memory polymer interlayers *Mater. Res. Express* **6** 115711
- [13] Su X, Wang Y and Peng X 2020 An anisotropic visco-hyperelastic model for thermally-actuated shape memory polymer-based woven fabric-reinforced composites *Int. J. Plast.* **129** 102697
- [14] Tan Q, Liu L, Liu Y and Leng J 2013 Post buckling analysis of the shape memory polymer composite laminate bonded with alloy film *Composites B* **53** 218–25
- [15] Guo X, Liu L, Zhou B, Liu Y and Leng J 2016 Constitutive model for shape memory polymer based on the viscoelasticity and phase transition theories *J. Intell. Mater. Syst. Struct.* **27** 314–23
- [16] Guo J, Liu J, Wang Z, He X, Hu L, Tong L and Tang X 2017 A thermodynamics viscoelastic constitutive model for shape memory polymers *J. Alloys Compd.* **705** 146–55
- [17] Sudarisman S and Davies I J 2008 Flexural failure of unidirectional hybrid fibre-reinforced polymer (FRP) composites containing different grades of glass fibre *Adv. Mater. Res.* **41–42** 357–62
- [18] Sudarisman S and Davies I J 2008 Influence of compressive pressure, vacuum pressure, and holding temperature applied during autoclave curing on the microstructure of unidirectional CFRP composites *Adv. Mater. Res.* **41–42** 323–8
- [19] Manders P W and Bader M G 1981 The strength of hybrid glass/carbon fiber composites *J. Mater. Sci.* **16** 2233–45
- [20] Yao J, Zhang T and Niu Y 2020 Effect of curing time on phase morphology and fracture toughness of PEK-C film interleaved carbon fiber/epoxy composite laminates *Compos. Struct.* **248** 112550
- [21] King R L 1989 Fibre-reinforced composites materials, manufacturing and design *Composites* **20** 172–3
- [22] Lee S H and Waas A M 1999 Compressive response and failure of fiber reinforced unidirectional composites *Int. J. Fract.* **100** 275–306
- [23] Wonderly C, Grenestedt J, Fernlund G and Căpus E 2005 Comparison of mechanical properties of glass fiber/vinyl ester and carbon fiber/vinyl ester composites *Composites B* **36** 417–26
- [24] Dong C and Davies I J 2014 Flexural and tensile strengths of unidirectional hybrid epoxy composites reinforced by S-2 glass and T700S carbon fibres *Mater. Des.* **54** 955–66
- [25] Dong C, Ranaweera-Jayawardena H A and Davies I J 2012 Flexural properties of hybrid composites reinforced by S-2 glass and T700S carbon fibres *Composites B* **43** 573–481
- [26] Dong C and Davies I J 2012 Optimal design for the flexural behavior of glass and carbon fiber reinforced polymer hybrid composites *Mater. Des.* **37** 450–7
- [27] Yan X and Cao S 2018 Structure and interfacial shear strength of polypropylene-glass fiber/carbon fiber hybrid composites fabricated by direct fiber feeding injection molding *Compos. Struct.* **185** 362–72
- [28] Hung P, Lau K, Cheng L, Leng J and Hui D 2018 Impact response of hybrid carbon/glass fiber reinforced polymer composites designed for engineering applications *Composites B* **133** 86–90
- [29] Li F, Scarpa F, Lan X, Liu Y, Leng J and Leng J 2019 Bending shape recovery of unidirectional carbon fiber reinforced epoxy-based shape memory polymer composites *Composites A* **116** 169–79
- [30] ASTM D3518 1995 Standard test method for in-plane shear response of polymer matrix composite materials by tensile test of a laminate *Annual Book ASTM*
- [31] ASTM D3039-01M 2003 Standard test method for tensile properties of polymer matrix composite materials *Annual Book ASTM Standards*
- [32] ASTM D790-07 2007 Standard test methods for flexural properties of unreinforced and reinforced plastics and electrical insulating materials *Annual Book ASTM Standards*
- [33] Kretsis G 1987 A review of the tensile, compressive, flexural and shear properties of hybrid fibre-reinforced plastics *Composites* **18** 13–23
- [34] Swolfs Y, Gorbatikh L and Verpoest I 2013 Stress concentrations in hybrid unidirectional fibre-reinforced composites with random fibre packings *Compos. Sci. Technol.* **85** 10–16
- [35] ASTM D5023-15 2015 Standard test method for plastics: dynamic mechanical properties: in flexure (three-point bending) *Annual Book ASTM*
- [36] Dong C and Davies I J 2015 Flexural strength of bidirectional hybrid epoxy composites reinforced by E glass and T700S carbon fibers *Composites B* **72** 65–71